

# Fe ion valence states and oxygen vacancies in the $\text{La}_{0.5}\text{Sr}_{0.5}\text{FeO}_{3-\gamma}$ ferrite under vacuum annealing

V. Sedykh<sup>a,\*</sup>, V. Rusakov<sup>b</sup>, O. Rybchenko<sup>a,c</sup>, A. Gapochka<sup>b</sup>, K. Gavrilicheva<sup>a,d</sup>, O. Barkalov<sup>a</sup>, S. Zaitsev<sup>a</sup>, V. Kulakov<sup>a</sup>

<sup>a</sup> Osipyan Institute of Solid State Physics, Russian Academy of Sciences, Chernogolovka, 142432, Russia

<sup>b</sup> Lomonosov Moscow State University, Moscow, 119991, Russia

<sup>c</sup> National Research University 'Higher School of Economics', HSE University, Moscow, Russia

<sup>d</sup> Bauman Moscow State Technical University, Moscow, Russia

## ARTICLE INFO

Handling Editor: Dr P. Vincenzini

**Keywords:**  
X-ray diffraction  
Spectroscopy  
Perovskites  
Ferrites

## ABSTRACT

The changes in the substituted  $\text{La}_{0.5}\text{Sr}_{0.5}\text{FeO}_{3-\gamma}$  orthoferrite under vacuum annealing in the temperature range of 200–650 °C have been studied by X-ray diffraction analysis, as well as Mössbauer and Raman spectroscopy. Annealing of the as-prepared ferrite with the rhombohedral structure ( $R\bar{3}c$ ) resulted in its transition to the cubic one ( $Pm\bar{3}m$ ) at 650 °C. In the as-prepared ferrite being paramagnetic at room temperature, Fe ions were detected in an averaged-valence state between  $\text{Fe}^{3+}$  and  $\text{Fe}^{4+}$ , which was not revealed with a decrease in the temperature down to 85 K. Gradual oxygen loss and an increase in the number of oxygen vacancies took place with an increase in the vacuum annealing temperature. Only  $\text{Fe}^{3+}$  ions were present in the ferrite at a vacuum annealing temperature above 500 °C. Several Zeeman sextets in the Mössbauer spectra associated with  $\text{Fe}^{3+}$  ions were resulted from the presence of oxygen vacancies and  $\text{Fe}^{4+}$  ions in the local environment of  $\text{Fe}^{3+}$  ions. The variations in the ratio of the valence states of Fe ions obtained from Mössbauer data depending on a vacuum annealing temperature allowed determining the content of oxygen in all the investigated samples. The contribution of  $\text{Fe}^{3+}$  ions that did not have  $\text{Fe}^{4+}$  ions and oxygen vacancies in their local environment was shown to increase with a vacuum annealing temperature from 12% (for the as-prepared sample) to 60% (for the sample annealed at 650 °C). On a whole, the process taking place under vacuum annealing can be characterized as a variation of the local environment of  $\text{Fe}^{3+}$  ions towards a decrease in its distortion. It was found that the width of the peaks of the Raman spectra decreased and their amplitude increased with an increase in the vacuum annealing temperature, which also demonstrated the improvement of the structural perfection of the samples.

## 1. Introduction

Perovskite-like oxides with  $\text{R}_{1-x}\text{A}_x\text{BO}_{3-\gamma}$ -type heterovalence substitution (where R is the rare-earth element, A is Ba, Ca, or Sr, and B is Fe, Mn, Co, or Ni) are promising materials due to their unusual electrical, magnetic, and catalytic properties [1,2]. They can be used as electrode materials for fuel elements, catalysts, chemical sensors, optoelectronic devices, and magnetic memory devices [3–7].

Transition metal ions in these systems have mixed-valence states, which provide high electron conductivity at room temperature [8]. Oxygen nonstoichiometry (the presence of oxygen vacancies) causes high oxygen ionic conductivity. A mixed valence state is formed to

compensate for charge disbalance; it can result from both the substitution of a trivalent element with divalent ions (A) and the formation of oxygen vacancies [9].

Magnetic properties of substituted ferrites that are part of this family result from the superexchange interactions including 3d electrons of transition metal ions and p oxygen orbitals [10]. In  $\text{LaFeO}_3$  that is multiferroic [11], Fe ions are in a trivalent state with an octahedral oxygen environment, in which oxygen octahedra have common vertices. According to Goodenough's theory [12], superexchange interaction between  $\text{Fe}^{3+}$  and  $\text{Fe}^{3+}$  cations is antiferromagnetic and stronger than that between  $\text{Fe}^{4+}$  and  $\text{Fe}^{3+}$ , as well as  $\text{Fe}^{4+}$  and  $\text{Fe}^{4+}$  ions.

When divalent  $\text{Sr}^{2+}$  substitutes for trivalent  $\text{La}^{3+}$  in  $\text{LaFeO}_3$ , the

\* Corresponding author. Osipyan Institute of Solid State Physics, Russian Academy of Sciences, Academician Osipyan 2, Chernogolovka, Moscow District, 142432, Russia.

E-mail address: [sedykh@issp.ac.ru](mailto:sedykh@issp.ac.ru) (V. Sedykh).

<https://doi.org/10.1016/j.ceramint.2023.05.105>

Received 2 February 2023; Received in revised form 23 April 2023; Accepted 10 May 2023

Available online 24 May 2023

0272-8842/© 2023 Elsevier Ltd and Techna Group S.r.l. All rights reserved.

structural and charge orderings are violated at a local level. This substitution results in the emergence of  $\text{Fe}^{4+}$  ions in the ferrite  $\text{La}_{1-x}\text{Sr}_x\text{FeO}_{3-y}$  structure and the formation of oxygen vacancies. This results in the weakening of an antiferromagnetic order. The Neel temperature  $T_N$  decreases with an increase in the Sr concentration [13–15].  $T_N$  is the highest in stoichiometric  $\text{LaFeO}_3$  ( $T_N \approx 740$  K [12,16]), while  $\text{SrFeO}_3$  containing only  $\text{Fe}^{4+}$  ions is ordered antiferromagnetically at  $T_N = 134$  K [17].

According to Ref. [18], the  $\text{La}_{1-x}\text{Sr}_x\text{FeO}_3$  ferrite has a rhombohedral structure in the range of  $x = 0.4 \div 0.5$ . The oxygen stoichiometry was reached under special annealing at high oxygen pressure. The  $\text{La}_{0.5}\text{Sr}_{0.5}\text{FeO}_{3-y}$  compound prepared at normal pressure (in the air) also has a rhombohedral structure [19,20], which transforms into the cubic perovskite lattice under heating as shown in Ref. [20].

Mössbauer spectroscopy is an effective method for the study of the valence states of Fe ions and the variation of their nearest oxygen environment in substituted ferrites. In these compounds, Mössbauer spectra of Fe ions with different valence states are composed of a few subspectra of the magnetic-ordered type. The substitution of an alkali-earth element for La leads to a decrease in the value of an effective magnetic field, while the emergence of oxygen vacancies changes an isomer shift [21,22].

A series of ferrites of rare-earth elements was studied in detail by Raman spectroscopy in Ref. [23]. Density functional theory calculations performed in Ref. [23] for  $\text{LaFeO}_3$  allowed assigning reliably the observed experimental peaks to the lattice vibration modes of the ferrite. In our earlier work on the study of the  $\text{La}_{0.67}\text{Sr}_{0.33}\text{FeO}_{3-\delta}$  ferrite [24], it was shown that a set of wide optical bands gradually appeared in the spectrum of the substituted ferrite under vacuum annealing with an increase in the annealing temperature. The position and intensity of these bands were similar to those of  $\text{LaFeO}_3$ . This makes Raman spectroscopy a very effective instrument in the investigation of structural changes in the ferrite under vacuum annealing.

In the present work, the changes in the structure and the valence states of Fe ions in the substituted  $\text{La}_{0.5}\text{Sr}_{0.5}\text{FeO}_{3-y}$  orthoferrite were studied under vacuum annealing using X-ray diffraction analysis, as well as Mössbauer and Raman spectroscopy.

## 2. Material and methods

A polycrystalline  $\text{La}_{0.5}\text{Sr}_{0.5}\text{FeO}_{3-y}$  sample was prepared in the air by a sol-gel method at  $1100^\circ\text{C}$  for 20 h using Sr, Fe, and La nitrates in a stoichiometric proportion and glycine as starting reagents. The details of the preparation procedure were described in Ref. [25]. After the synthesis, the sample and the furnace were cooled down slowly to room temperature. Then, the samples were annealed in vacuum ( $10^{-3}$  Torr) at  $200$ – $550^\circ\text{C}$  for 4 h to decrease the oxygen concentration in the lattice. The last sample of this series was annealed at  $650^\circ\text{C}$  for 10 h to finally stabilize the state.

The structural characterization of the polycrystalline samples was carried out at room temperature on a Rigaku SmartLab SE diffractometer using  $\text{CuK}\alpha$  radiation. The Powder Cell 2.4 and Match3 software packages were used for the phase analysis and determination of the structural parameters.

The Mössbauer measurements of the polycrystalline samples were performed at room temperature and at 85 K on a CM 1101 spectrometer operating in a constant acceleration mode. The radioactive source was  $^{57}\text{Co}$  (Rh). The spectra were fitted and analyzed using model fitting and the distribution of hyperfine spectral parameters by the SpectrRelax program [26].

The Raman spectra were recorded with a Princeton Instruments HRS 500 spectrometer equipped with a liquid nitrogen-cooled charge-coupled device detector and a grating of 1200 grooves/mm. The samples were irradiated in a back-scattering geometry at room temperature with a 532 nm KLM-532 nm DPSS laser. The laser power at the sample was  $\sim 5$  mW. A 20x Plan Apo Mitutoyo objective was used to

focus the laser beam to a spot of  $\sim 3$   $\mu\text{m}$  in size and collect the scattered light. The spectral width of the setup was  $200$   $\text{cm}^{-1}$ . The spectral resolution in the studied spectral range was  $\approx 1$   $\text{cm}^{-1}$  with an absolute accuracy of  $\pm 1$   $\text{cm}^{-1}$ .

## 3. Results and discussion

### 3.1. X-ray diffraction data

The lines of all the X-ray diffraction patterns of the series, except for that of the sample annealed at  $650^\circ\text{C}$ , are strongly broadened (see the right panel of Fig. 1). This may be associated with both a small size of crystallites and heterogeneous oxygen distribution over the sample. This strong broadening results in the overlap of diffraction lines and hinders the identification of the structure. However, the detailed consideration of the shape of the curves describing the total intensity of the separated line groups helps us to choose the space group with more certainty.

The X-ray diffraction pattern of the as-prepared (synthesized)  $\text{La}_{0.5}\text{Sr}_{0.5}\text{FeO}_{3-y}$  sample (Fig. 1) was well described by the rhombohedral unit cell with the space group  $R\bar{3}c$  and lattice parameters  $a = 5.511$  (2)  $\text{\AA}$ ,  $c = 13.437$ (4)  $\text{\AA}$  in hexagonal axes ( $a = 5.494$ (2)  $\text{\AA}$  and  $\alpha = 60.20$  (1) $^\circ$ ) for the rhombohedral unit cell). The cubic ( $Pm\bar{3}m$ ) and orthorhombic ( $Pbnm$ ) structures were also considered; however, they yielded worse agreement with the experimental data. The diffraction patterns of all the studied samples are similar. This means that the evolution of the ferrite structure occurs by small successive rearrangements during vacuum annealing. The structure remains rhombohedral with increasing the vacuum annealing temperature  $T_{\text{ann}}$ , except for the sample annealed at  $650^\circ\text{C}$ ; only the unit cell parameters change monotonically. In particular, the angle  $\alpha$  decreases from  $60.20^\circ$  to  $60.00^\circ$  (Fig. 2a). This means that the rhombohedral distortion of the pseudocubic unit cell is reduced with a decrease in the oxygen concentration and disappears in the sample annealed at  $650^\circ\text{C}$  for 10 h (Fig. 2a). The X-ray diffraction pattern of this sample (Fig. 1c) is well described by the cubic unit cell ( $Pm\bar{3}m$ ) with  $a = 3.914$ (1)  $\text{\AA}$ .

It is convenient to use the value of volume per one pseudocubic perovskite cell to describe the evolution of the ferrite structure. The dependence of the pseudocubic unit cell volume on the vacuum annealing temperature is shown in Fig. 2b. The unit cell volume continuously increases with annealing temperature within the range of

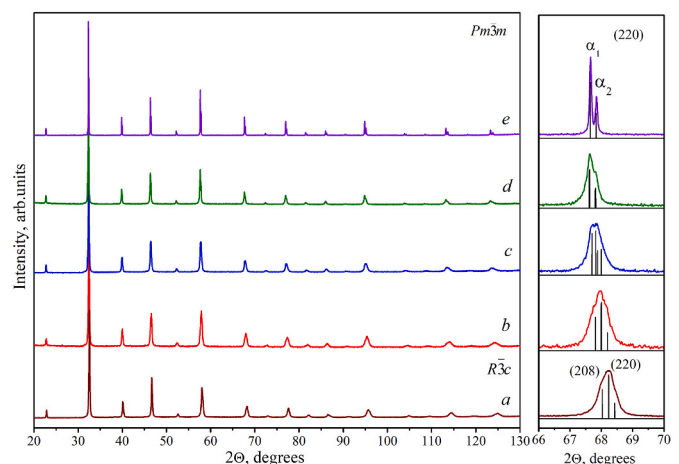


**Fig. 1.** X-ray diffraction patterns of the  $\text{La}_{0.5}\text{Sr}_{0.5}\text{FeO}_{3-\delta}$  ferrites. Main panel: (a) the pattern of the as-prepared  $\text{La}_{0.5}\text{Sr}_{0.5}\text{FeO}_{2.84}$ ; the patterns of the samples annealed in vacuum at (b)  $300^\circ\text{C}$ , (c)  $400^\circ\text{C}$ , (d)  $550^\circ\text{C}$ , (e)  $650^\circ\text{C}$  for 10 h. (a)–(d) the  $R\bar{3}c$  phase and (e) the  $Pm\bar{3}m$  phase. The right panel demonstrates the fragments of the experimental patterns on a larger scale. The Miller indexes of the reflections are given in brackets. The intensities of the X-ray patterns in the right panel are not normalized.

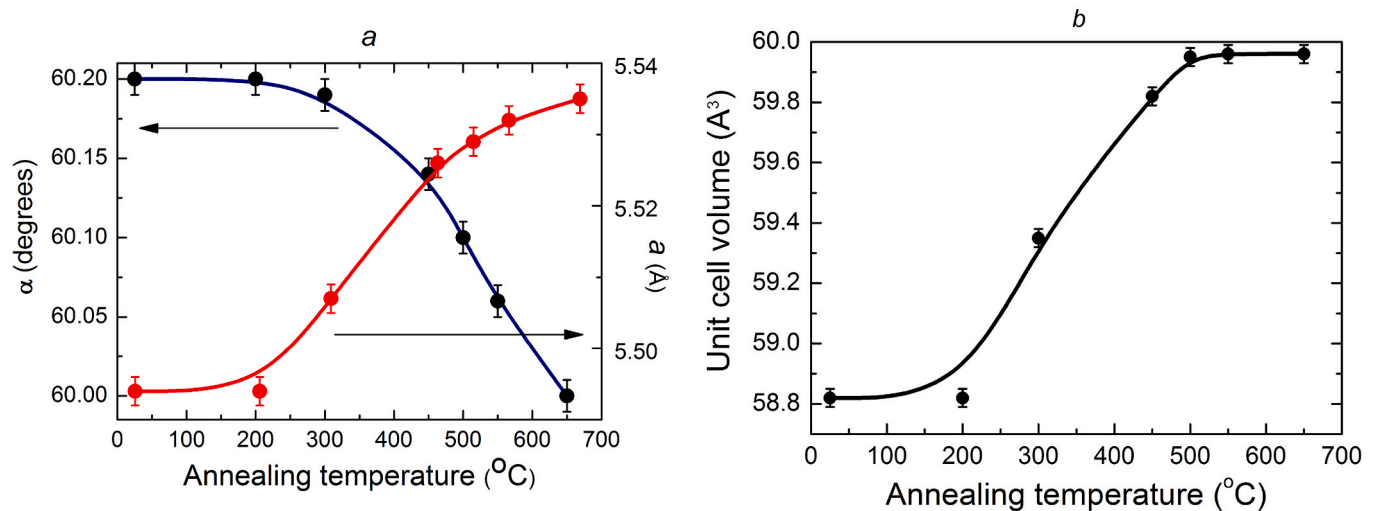


Fig. 2. (a) Parameters of the rhombohedral unit cell ( $R\bar{3}c$ ) and (b) unit cell volume of the  $\text{La}_{0.5}\text{Sr}_{0.5}\text{FeO}_{3-\gamma}$  ferrite plotted as a function of the vacuum annealing temperature. The lines drawn through the data points are guides for the eye.

200–500 °C, and this process is leveled at higher temperatures. In the literature, this is associated with a decrease in the concentration of oxygen in the lattice, which operates as a contractive factor [27,28], or with the substitution of  $\text{Fe}^{3+}$  for  $\text{Fe}^{4+}$  ions that have a significantly larger ionic radius [20].

The X-ray diffraction patterns of the samples annealed at 300 °C and 400 °C were also well described by the orthorhombic lattice ( $Pbnm$ ) and one annealed at 550 °C by the cubic lattice ( $Pm\bar{3}m$ ); however, it is very difficult to make an unambiguous choice because of the strong broadening of the diffraction lines.

### 3.2. Mössbauer spectroscopy

#### 3.2.1. Room temperature measurements

The room-temperature Mössbauer spectra of the as-prepared  $\text{La}_{0.5}\text{Sr}_{0.5}\text{FeO}_{3-\gamma}$  sample and those annealed in vacuum at  $T_{\text{ann}} = 300$  and 650 °C are shown in Fig. 3. The distribution  $p(H_{\text{hf}})$  of a hyperfine magnetic field  $H_{\text{hf}}$  was reconstructed for each spectrum taking into account a possible paramagnetic contribution described by the quadrupole doublet.

When reconstructing  $p(H_{\text{hf}})$ , the presence of linear correlation between a hyperfine magnetic field and the isomer shift  $\delta$  of the spectrum was suggested at the desired average value of the quadrupole splitting  $\varepsilon$ . The  $T_{\text{ann}}$  dependence of the relative areas and hyperfine parameters of Mössbauer subspectra are shown in Fig. 4 for the  $\text{La}_{0.5}\text{Sr}_{0.5}\text{FeO}_{3-\gamma}$  samples as compared to the corresponding data for pure  $\text{LaFeO}_3$ .

The as-prepared sample is a paramagnet (Fig. 3a) and is described by a quadrupole doublet. The subspectrum of the magnetic-ordered type arises in the spectrum of the sample annealed at 200 °C; its contribution increases with increasing  $T_{\text{ann}}$  (Fig. 3b and 4a). The presence of several low-intensity maxima in the distribution  $p(H_{\text{hf}})$  (Fig. 3b) can be associated with both statistic variations in the magnetic part of the spectrum and a local inhomogeneity for Fe ions. This inhomogeneity is caused by the presence of different numbers of oxygen vacancies and Fe ions with different valence states in the structure. The quadrupole doublet is almost absent in the spectra at  $T_{\text{ann}} \geq 450$  °C (Fig. 3c and 4a). As noted above, the substitution of Sr ions for La in  $\text{LaFeO}_3$  results in the appearance of  $\text{Fe}^{4+}$  ions in addition to  $\text{Fe}^{3+}$  ions. The values of the isomer shifts of the quadrupole doublets  $\delta = 0.14 \div 0.18$  mm/s for the as-prepared sample and those annealed up to 450 °C indicate that a part of Fe ions is in an averaged-valence state, i.e., is with a fractional oxidation degree between 3+ and 4+ (Fig. 4c). This averaged-valence state of Fe ions is due to the fast (with a characteristic time of  $<10^{-8}$  s)

electron transfer between  $\text{Fe}^{3+}$  and  $\text{Fe}^{4+}$  ions at room temperature; therefore,  $\text{Fe}^{4+}$  ions are not detected in the room-temperature Mössbauer spectra [15,21,29].

According to the average values  $\delta_{\text{aver}}(p(H_{\text{hf}})) \sim 0.30$  mm/s and the values in the maximum of the distribution of isomer shifts  $\delta_{\text{max}}(p(H_{\text{hf}})) \sim 0.34$  mm/s (Fig. 4c) for magnetic-ordered subspectra of the samples annealed at 200 °C and higher, Fe ions corresponding to these values are in a trivalent state,  $\text{Fe}^{3+}$ . For  $\text{Fe}^{3+}$  ions, the broadened distribution  $p(H_{\text{hf}})$  of a hyperfine magnetic field  $H_{\text{hf}}$  is caused by local heterogeneity in the environment of Fe ions, namely, by the presence of oxygen vacancies and different valence states of Fe ions in the structure.

The area of the quadrupole doublet  $S(\text{doublet})$  significantly decreases with increasing  $T_{\text{ann}}$  (Fig. 4a), which is equivalent to a decrease in the number of Fe ions in an averaged-valence state. This leads to a decrease in the local heterogeneity degree in the nearest environment of  $\text{Fe}^{3+}$  ions and, as a consequence, to a decrease in the width of the distribution  $p(H_{\text{hf}})$ . Beginning from  $T_{\text{ann}} = 450$  °C, Fe ions in an averaged-valence state are almost absent. In the annealing temperature range of 500–650 °C,  $H_{\text{max}}(p(H_{\text{hf}}))$  and  $\delta_{\text{max}}(p(H_{\text{hf}}))$  reach their maximum values and the width of distribution  $p(H_{\text{hf}})$  reaches its minimum values, which approach the values for  $\text{LaFeO}_3$  (Fig. 4). The presence of two clear peaks in the distribution  $p(H_{\text{hf}})$  (Fig. 3c) for the sample annealed at 650 °C testifies to the existence of only two dominating contributions to the spectrum. Their appearance becomes understandable after the analysis of the 85-K Mössbauer spectra, which is given below. The largest value of quadrupole splitting  $\varepsilon$  of  $\sim 0.18$  mm/s is observed for the doublet of the as-prepared sample, which decreases almost to zero at 400 °C with increasing  $T_{\text{ann}}$  and does not change at higher annealing temperatures. The average value of  $\varepsilon_{\text{aver}}(p(H_{\text{hf}}))$  for the  $p(H_{\text{hf}})$  distribution is near zero for all annealing temperatures. The value of  $\varepsilon$  for  $\text{LaFeO}_3$  is 0.036(1) mm/s.

An increase in the number of oxygen vacancies should lead to the distortion of an oxygen environment of Fe ions and, consequently, to an increase in the  $\varepsilon$  value of the Mössbauer spectra. One can suppose that the near-zero  $\varepsilon$  value is related to the high oxygen mobility [8], an increase in the perovskite cell volume with increasing  $T_{\text{ann}}$ , and possible redistribution of oxygen ions for the creation of a more symmetrical oxygen environment of Fe ions.

#### 3.2.2. Low temperature (85 K) measurements

The 85-K Mössbauer spectra of the  $\text{La}_{0.5}\text{Sr}_{0.5}\text{FeO}_{3-\gamma}$  samples are a set of several subspectra in the form of Zeeman sextets. One of them, which has the smallest isomer shift and a hyperfine magnetic field, can be

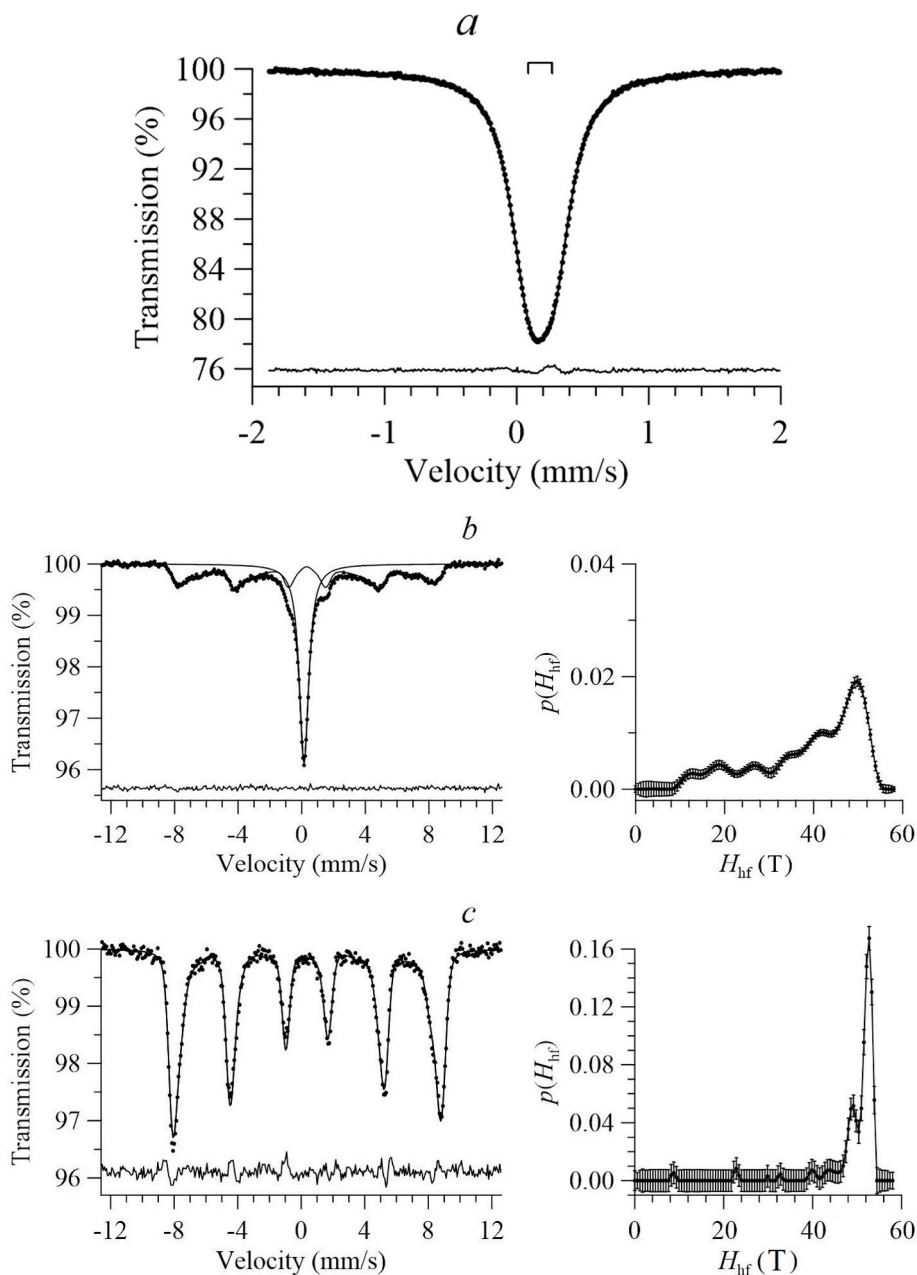
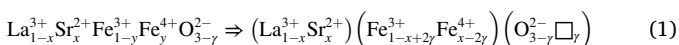


**Fig. 3.** The results of Mössbauer spectrum fitting of the as-prepared sample (a) and the results of the reconstruction of the distribution  $p(H_{hf})$  of a hyperfine magnetic field  $H_{hf}$  taking into account the paramagnetic contribution for the Mössbauer spectra of the  $\text{La}_{0.5}\text{Sr}_{0.5}\text{FeO}_{3-\gamma}$  samples annealed in vacuum at 300 °C (b) and 650 °C (c). The thick solid line is a resultant fitting curve. The difference spectra between the experimental points and the calculated curve are shown at the bottom of each spectrum.

associated with  $\text{Fe}^{4+}$  ions, while the others can be attributed to  $\text{Fe}^{3+}$  ions (Fig. 5).

The presence of several subspectra for  $\text{Fe}^{3+}$  ions in each spectrum of the substituted ferrite is associated with the possible different numbers of oxygen vacancies and  $\text{Fe}^{4+}$  ions in the nearest environment of  $\text{Fe}^{3+}$  ions, i.e., with the formation of a heterogeneous local environment. Vacuum annealing of the as-prepared sample increases the number of oxygen vacancies and, as shown in Fig. 5, decreases the number of  $\text{Fe}^{4+}$  ions; and, thus, the areas of the subspectra for  $\text{Fe}^{3+}$  ions are redistributed.

Based on the electroneutrality condition, the crystal-chemical formula of  $\text{La}_{1-x}\text{Sr}_x\text{FeO}_{3-\gamma}$  can be written as:



where  $x$ ,  $y = x - 2\gamma$ , and  $\gamma = (x - y)/2$  are the number of  $\text{Sr}^{2+}$  and  $\text{Fe}^{4+}$  ions and oxygen vacancies ( $\square$ ) per formula unit of the ferrite, respectively. For  $\text{La}_{0.5}\text{Sr}_{0.5}\text{FeO}_{3-\gamma}$ ,  $\gamma = (0.5 - y)/2$ .

The presence of a  $\text{Fe}^{4+}$  ion in the nearest cation environment of a  $\text{Fe}^{3+}$  ion results in the weakening of the superexchange interaction  $\text{Fe}^{3+}-\text{O}^{2-}-\text{Fe}^{4+}$ , while the emergence of an oxygen vacancy in the nearest anion environment of a  $\text{Fe}^{3+}$  ion leads to the breaking of the exchange bond. These effects decrease a hyperfine magnetic field  $H_{hf}$  and change the value of the isomer shift of the spectrum [30]. When fitting the Mössbauer spectra, additive changes in the hyperfine magnetic field and the isomer shift of  $\text{Fe}^{3+}$  ion subspectra were suggested, which were identical for the vacancy and  $\text{Fe}^{4+}$  ion when the number of either breaking or weakening of the exchange bonds ( $m$ ) was increased:

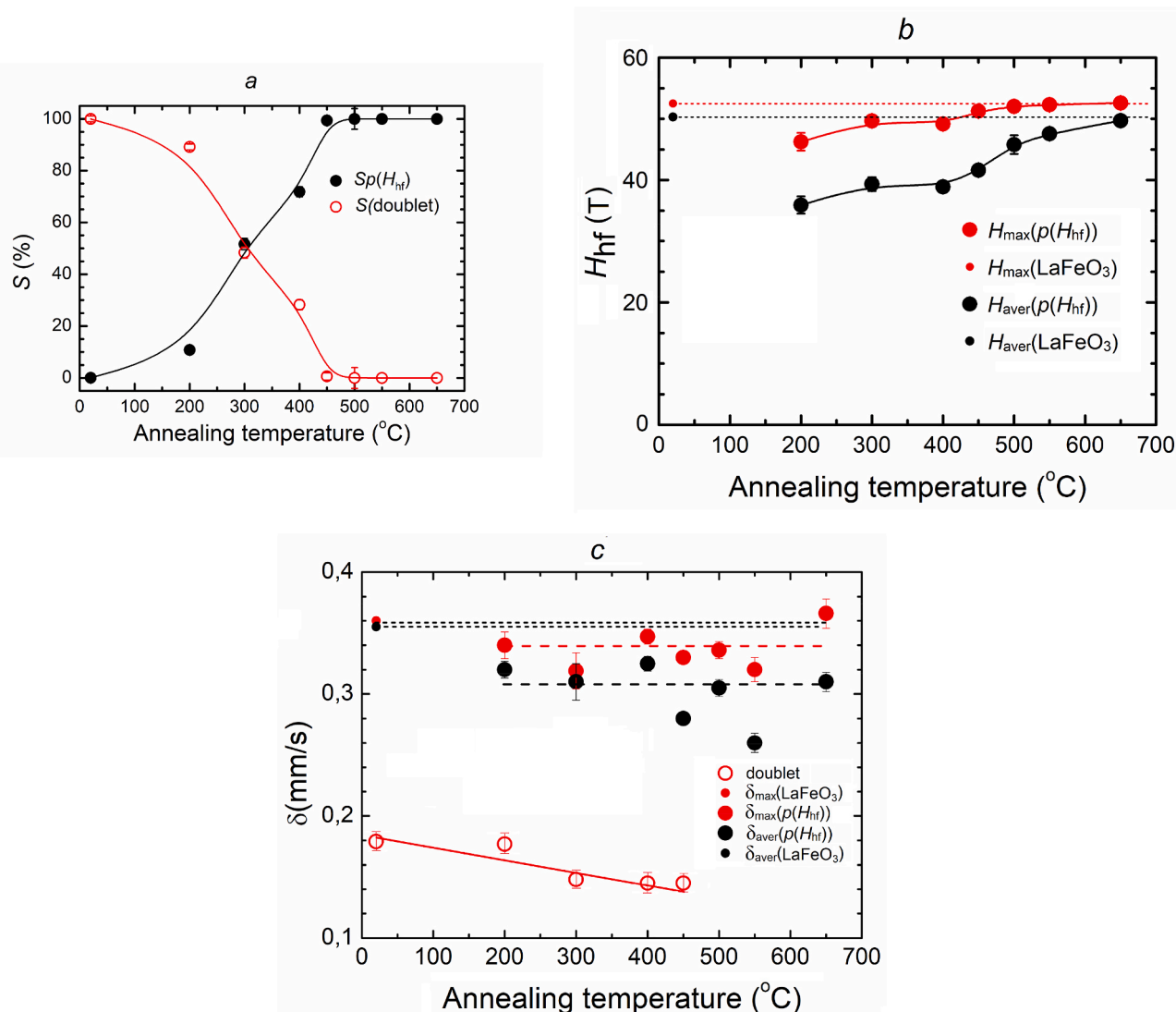


**Fig. 4.** The  $T_{\text{ann}}$  dependence of (a) the relative areas of the quadrupole doublet  $S(\text{doublet})$  and the subspectrum of the magnetic-ordered type corresponding to the distribution  $p(H_{\text{hf}})$ ; (b,c) hyperfine parameters of the subspectra of the  $\text{La}_{0.5}\text{Sr}_{0.5}\text{FeO}_{3-\gamma}$  samples: the average values ( $H_{\text{aver}}$ ,  $\delta_{\text{aver}}$ ) and the values in the maximum ( $H_{\text{max}}$ ,  $\delta_{\text{max}}$ ) of the distribution. The corresponding values for  $\text{LaFeO}_3$  are shown for comparison. The lines drawn through the data points are guides for the eye.

$$H_{\text{hf}}(\text{Fe}^{3+}; m) = H_{\text{hf}}(\text{Fe}^{3+}; 0) - m\Delta H_{\text{hf}}(\text{Fe}^{3+}) \quad (2)$$

$$\delta(\text{Fe}^{3+}; m) = \delta(\text{Fe}^{3+}; 0) + m\Delta\delta(\text{Fe}^{3+}) \quad (3)$$

Here  $H_{\text{hf}}(\text{Fe}^{3+}; 0)$  and  $\delta(\text{Fe}^{3+}; 0)$  are the values of the hyperfine magnetic field and the isomer shift for the subspectrum of  $\text{Fe}^{3+}$  ions with six exchange bonds when there are no oxygen vacancies or  $\text{Fe}^{4+}$  ions in the nearest  $\text{Fe}^{3+}$  environment, and  $\Delta H_{\text{hf}}(\text{Fe}^{3+})$  and  $\Delta\delta(\text{Fe}^{3+})$  are the changes in the hyperfine magnetic field and the isomer shift when either breaking or weakening of one exchange bond takes place.

For simplicity, the value of the quadrupole splitting  $\epsilon$  was suggested to be the same for all subspectra of  $\text{Fe}^{3+}$  ions. In the general case, their positions in the crystallographic positions relative to  $\text{Fe}^{3+}$  ions and each other can differ at the same  $m$  value, which results in different  $\epsilon$  values.

The fitting of the spectra was performed taking into account the possible number of oxygen vacancies ( $\gamma$ ) and  $\text{Fe}^{4+}$  ions ( $y$ ) up to obtaining the best difference spectrum. It corresponded to five subspectra for  $\text{Fe}^{3+}$  ions and one subspectrum for  $\text{Fe}^{4+}$  ions (Fig. 5). The  $T_{\text{ann}}$  dependencies of the relative areas of the  $\text{Fe}^{4+}$  subspectrum and the sum of all subspectra for  $\text{Fe}^{3+}$  ions obtained from the model fitting of the experimental Mössbauer spectra are shown in Fig. 6a. The relative area of the subspectrum associated with  $\text{Fe}^{4+}$  is maximum for the as-prepared sample. Its area decreases with increasing  $T_{\text{ann}}$  and

approaches zero at  $T_{\text{ann}} = 650$  °C. In this case, the greatest changes take place until  $T_{\text{ann}} = 500$  °C, while at a higher temperature the areas almost do not change (Fig. 6a). The hyperfine parameters of the  $\text{Fe}^{4+}$  subspectrum were taken from the results of the fitting of the as-prepared sample spectrum and fixed since its contribution to the experimental spectrum was small at high annealing temperatures.

As was mentioned above, a superexchange interaction between Fe ions is weakened in lanthanum orthoferrites when Sr is substituted for La, i.e., when  $\text{Fe}^{4+}$  ions and oxygen vacancies appear. The contributions of the subspectra for different  $\text{Fe}^{3+}$  states are redistributed with increasing  $T_{\text{ann}}$  (Fig. 6b). The relative area of the subspectrum  $S(\text{Fe}^{3+}; 0)$  for  $\text{Fe}^{3+}$  ions with six exchange bonds  $\text{Fe}^{3+}-\text{O}^{2-}-\text{Fe}^{3+}$  ( $m = 0$ ) significantly increases from the minimum value of 12% for the as-prepared sample to ~60% for the sample annealed at 650 °C in vacuum. The second significant contribution is given by the subspectrum of  $\text{Fe}^{3+}$  ions for  $m = 1$ . Its area  $S(\text{Fe}^{3+}; 1)$  increases in the  $T_{\text{ann}}$  range of 200 ÷ 300 °C; then, it almost does not change and reaches ~30% at 650 °C. The areas of the subspectra of  $\text{Fe}^{3+}$  ions decrease for  $m = 2, 3, 4$  (Fig. 6b). This means that almost two principal subspectra of  $\text{Fe}^{3+}$  ions for  $m = 0$  and 1 with the most perfect local environment remain at 650 °C. These two principal contributions are manifested in the distribution of hyperfine

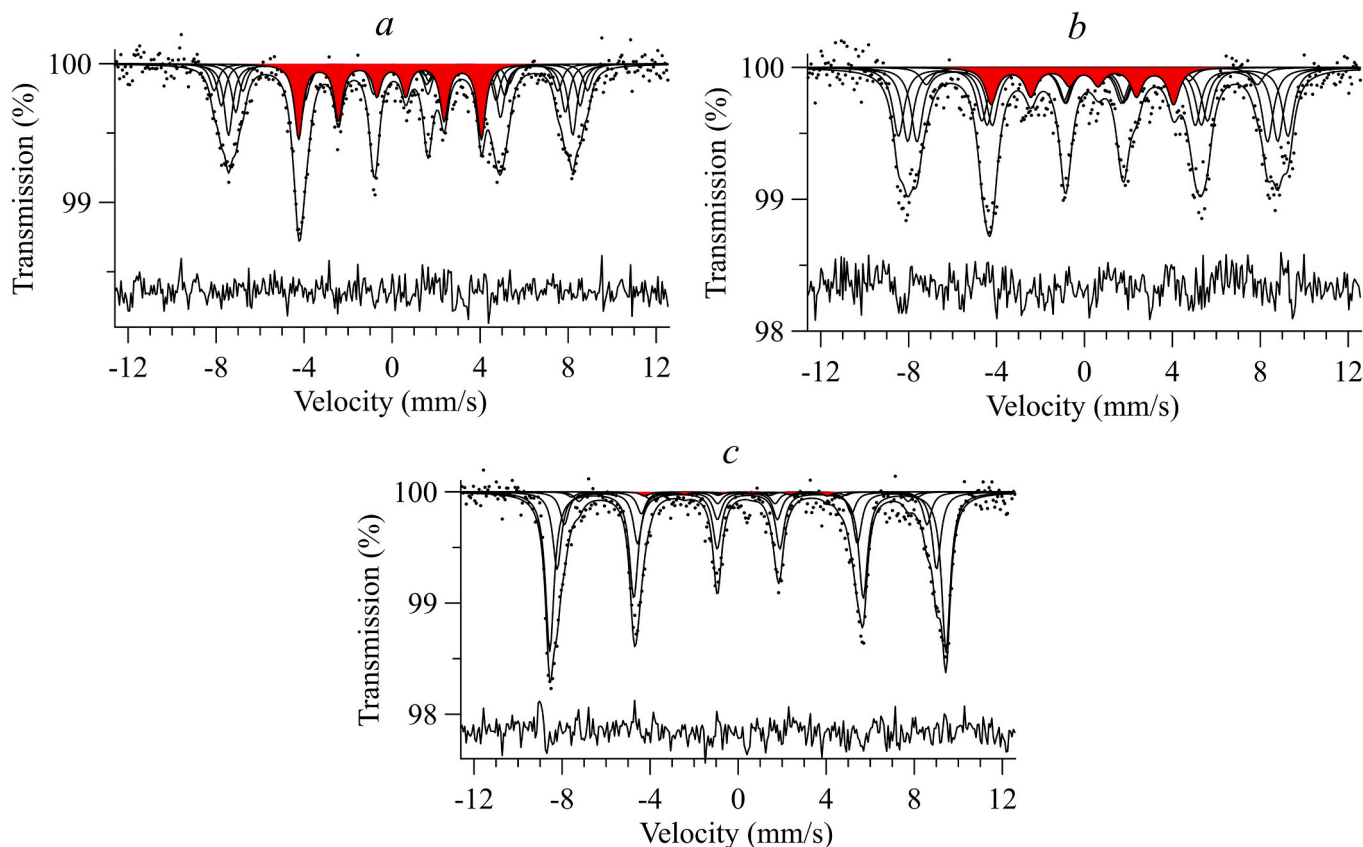


**Fig. 5.** The results of the model fitting of 85-K Mössbauer spectra of the  $\text{La}_{0.5}\text{Sr}_{0.5}\text{FeO}_{3-\gamma}$  samples: as-prepared (a) and annealed in vacuum at 300 (b) and 650 °C (c). The subspectrum of  $\text{Fe}^{4+}$  ions is marked with red. The difference spectra (deviation of the experimental spectra from the calculated envelope ones) are shown at the bottom of each spectrum. (For interpretation of the references to colour in this figure legend, the reader is referred to the Web version of this article.)

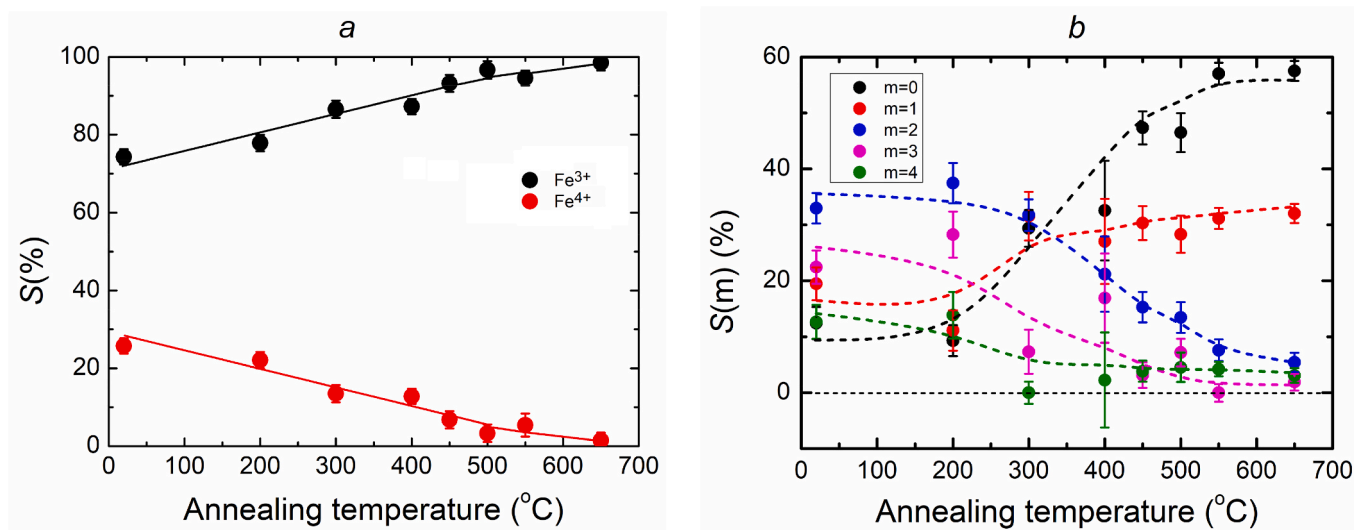


**Fig. 6.** The  $T_{\text{ann}}$  dependencies of the relative areas of the subspectra: (a) for all  $\text{Fe}^{3+}$  and  $\text{Fe}^{4+}$  ions and (b) for  $\text{Fe}^{3+}$  ions, in the nearest environment of which  $m = 0, 1, 2, 3, 4$  either breaking or weakening of exchange couplings occurred. The Mössbauer parameters correspond to the 85-K spectra. The lines drawn through the data points are guides for the eye.

magnetic fields obtained at room temperature (Fig. 3c). As a whole, this process can be interpreted as a variation in the local environment of  $\text{Fe}^{3+}$  ions towards a decrease in its distortion.

A few interdependent processes occur in a crystal lattice under vacuum annealing: an oxygen ion moves away with the vacancy formation, the valence state of Fe ions changes, and oxygen ions are

redistributed over vacant positions to minimize lattice distortions. To comply with the electric neutrality conditions, in the substituted ferrite a  $\text{Fe}^{4+}$  ion must be in close proximity to  $\text{Sr}^{2+}$  to compensate for a negative charge. If an oxygen ion is removed from its nearest environment under vacuum annealing, an oxidation degree changes from 4+ to 3+. Moreover, one oxygen ion moving away (addition of one vacancy) leads to

the disappearance of two  $\text{Fe}^{4+}$  ions in the region under consideration. Thus, there is a correlation between the arrangement of an oxygen vacancy and that of a  $\text{Fe}^{4+}$  ion; in addition, their common arrangement is related to the distribution of Sr and La ions. The presence of this correlation in the  $\text{La}_{1-x}\text{Sr}_x\text{FeO}_{3-\gamma}$  compounds is shown in Refs. [13,19,31–33].

Assuming the recoil-free fraction for  $\text{Fe}^{3+}$  and  $\text{Fe}^{4+}$  to be the same, the numbers of  $\text{Fe}^{4+}$  ions ( $y = I(\text{Fe}^{4+})$ ), oxygen vacancies ( $\gamma = (x - y)/2$ ), and oxygen anions ( $3 - \gamma$ ) per formula unit can be determined (1) from the relative areas of the subspectra when the number of  $\text{Sr}^{2+}$  ions ( $x$ ) is fixed. The  $T_{\text{ann}}$  dependencies of the number of oxygen vacancies ( $\gamma$ ) and oxygen ions ( $3 - \gamma$ ) are demonstrated in Fig. 7. With increasing  $T_{\text{ann}}$ , the number of vacancies in the sample increases from 0.12(1) to 0.24(1) and, correspondingly, the number of oxygen anions decreases from 2.88 (1) to 2.76(1).

Assuming the linear dependence of the hyperfine parameters of the subspectra of  $\text{Fe}^{3+}$  ions on the number  $m$  of breaking or weakening of the exchange bonds (see (2) and (3)), the values of  $H_{\text{hf}}(\text{Fe}^{3+};0)$  and  $\delta(\text{Fe}^{3+};0)$  for the subspectrum of  $\text{Fe}^{3+}$  ions and the changes in the hyperfine magnetic field  $\Delta H_{\text{hf}}(\text{Fe}^{3+})$  and the isomer shift  $\Delta\delta(\text{Fe}^{3+})$  under either breaking or weakening of one exchange bond are determined for all the samples as a result of the model fitting of the spectra (Fig. 8). The hyperfine parameters of the subspectra of  $\text{Fe}^{3+}$  and  $\text{Fe}^{4+}$  ions obtained for  $\text{La}_{0.5}\text{Sr}_{0.5}\text{FeO}_{3-\gamma}$  weakly depend on  $T_{\text{ann}}$ . The values of  $H_{\text{hf}}(\text{Fe}^{3+};0)$  and  $\delta(\text{Fe}^{3+};0)$  are close to the corresponding values of  $H_{\text{hf}}$  and  $\delta$  for  $\text{LaFeO}_3$ , in which all  $\text{Fe}^{3+}$  ions participate in all six exchange bonds. The average values of  $\Delta H_{\text{hf}}(\text{Fe}^{3+})$  and  $\Delta\delta(\text{Fe}^{3+})$  are 2.3(3) T and 0.03(3) mm/s, respectively. The average values of the quadrupole splitting  $\varepsilon$  of the subspectrum components are small and near-zero for  $\text{Fe}^{3+}$  ions and negative,  $\sim -0.03$  mm/s, for  $\text{Fe}^{4+}$  ions.

The values  $H_{\text{hf}}(\text{Fe}^{4+}) = 25.7(1)$  T and  $\delta(\text{Fe}^{4+}) = -0.063(11)$  mm/s obtained for the spectrum of  $\text{Fe}^{4+}$  ions in the as-prepared sample and measured at 85 K agree well with the data for  $\text{Fe}^{4+}$  in  $\text{La}_{0.8}\text{Sr}_{0.4}\text{Fe}_{0.7}\text{Al}_{0.3}\text{O}_{3-\delta}$  [34]. The value of the isomer shift for the possible mixed charge state of Fe ions at 85 K can be estimated by using the values of isomer shifts and the relative areas of the subspectra for  $\text{Fe}^{3+}$  (+0.40 mm/s,  $\sim 70\%$ ) and  $\text{Fe}^{4+}$  (−0.06 mm/s,  $\sim 30\%$ ) ions obtained at 85 K (Figs. 8b and 6a); it is  $\sim -0.26$  mm/s. Taking into account a decrease in  $\delta$  of the spectrum by  $\sim 0.1$  mm/s with an increase in the temperature up to room one, the  $\delta$  value for the observed averaged charge state of a Fe ion

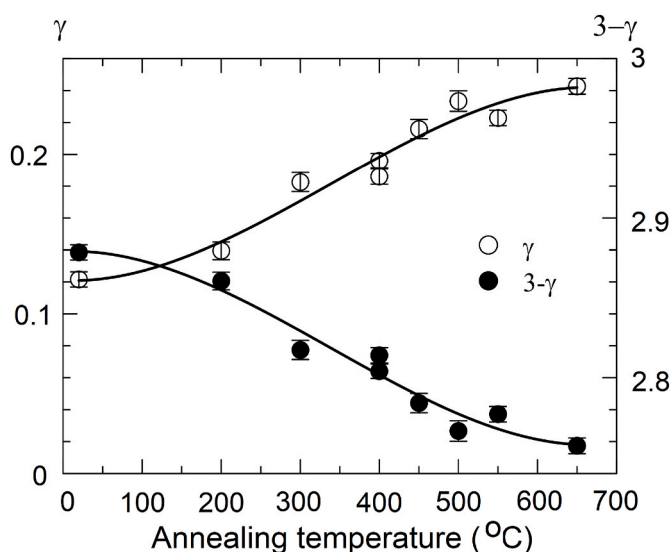


Fig. 7. The  $T_{\text{ann}}$  dependencies of the number of oxygen vacancies ( $\gamma$ ) and oxygen ions ( $3 - \gamma$ ) per formula unit in the  $\text{La}_{0.5}\text{Sr}_{0.5}\text{FeO}_{3-\gamma}$  ferrite. The Mössbauer parameters correspond to the 85-K spectra. The lines drawn through the data points are guides for the eye.

at room temperature is  $\sim 0.16$  mm/s, which corresponds well to the experimental value of 0.179(1) mm/s obtained at room temperature for the quadrupole doublet (Fig. 4c).

### 3.3. Raman spectroscopy

The characteristic Raman spectra of the samples annealed in vacuum at  $400 \div 650$  °C for 4 h are shown in Fig. 9. Seven broad optical bands are resolved in the spectra. An increase in the annealing temperature results in a pronounced decrease in the peak linewidth and an increase in the signal to the noise ratio. Both experimental facts indicate the improvement of the homogeneity of the samples and their crystalline structure upon the annealing process. As shown by the vertical bars in Fig. 9, the most intensive peaks in the spectra demonstrate a pronounced shift to higher frequencies when increasing the annealing temperature. An increase in the annealing time at 650 °C from 4 to 10 h does not lead to any detectable change in the Raman spectrum (compare the two lowest spectra in Fig. 9).

The frequency range of the spectra presented in Fig. 9 can be divided into two parts. The low-frequency bands (below  $1000 \text{ cm}^{-1}$ ) correspond to the phonon-like vibrations, while the high-frequency ones (above  $1000 \text{ cm}^{-1}$ ) are caused presumably by magnons of the ferrite antiferromagnetic sublattices since, according to the calculations of Weber et al. [23], no phonon-like vibrations in the parent  $\text{LaFeO}_3$  ferrite have frequencies higher than  $650 \text{ cm}^{-1}$ .

The Raman spectra of the La–Sr ferrites with Fe ions in a  $\text{Fe}^{3+}$  oxidation state are presented in Fig. 10. The spectra for  $\text{La}_{0.67}\text{Sr}_{0.33}\text{FeO}_{2.84}$  and  $\text{LaFeO}_3$  were taken from Ref. [24]. Successive substitution of La atoms with Sr ones results in the transformation of the orthorhombic lattice for pure  $\text{LaFeO}_3$  to the cubic perovskite one for  $\text{La}_{0.5}\text{Sr}_{0.5}\text{FeO}_{2.76}$ . The introduction of a divalent Sr atom causes the formation of oxygen vacancies in the ferrite structure, as shown by Mössbauer spectroscopy. As demonstrated recently in Ref. [23], for pure  $\text{LaFeO}_3$  the vibration modes in the frequency range of  $250 \div 650 \text{ cm}^{-1}$  are attributed only to the vibrations of Fe and oxygen atoms that form double-centered or multi-centered chemical bonds or even the vibrations of the  $\text{FeO}_6$  octahedra as a whole. Thus, the pronounced high-frequency shift observed in the range of  $600 \div 650 \text{ cm}^{-1}$  is caused by an increase in the number of oxygen vacancies. A similar shift was found also for the high-frequency magnon band of the spectra (see the inset of Fig. 10).

The Raman spectra of the annealed  $\text{La}_{1-x}\text{Sr}_x\text{FeO}_{3-\gamma}$  samples consist of several broadened bands. Their positions and relative intensities are similar to those of the peaks in the  $\text{LaFeO}_3$  spectrum. This analogy allowed associating the observed bands with the vibrations of two-, three-, and multi-centered Fe–O chemical bonds. In substituted  $\text{La}_{1-x}\text{Sr}_x\text{FeO}_{3-\gamma}$ , a noticeable shift towards  $\sim 690 \text{ cm}^{-1}$  is observed for the “breathing” mode of the  $\text{FeO}_6$  octahedron, as compared to the band at  $\sim 630 \text{ cm}^{-1}$  in stoichiometric  $\text{LaFeO}_3$ . According to the X-ray results of the present work, this shift is due to that the unit cell volume in the substituted  $\text{La}_{0.5}\text{Sr}_{0.5}\text{FeO}_{3-\gamma}$  ferrite is smaller by  $\sim 1\%$  as compared to that in  $\text{LaFeO}_3$  [32].

A wide band at frequencies higher than  $1000 \text{ cm}^{-1}$  in the ferrite spectrum is possibly due to two-magnon scattering. Its position and structure are similar to the two-magnon peaks of  $\text{LaFeO}_3$  and other La–Sr ferrites [35–38], which allows anticipating an antiferromagnetic ordering type for the  $\text{La}_{1-x}\text{Sr}_x\text{FeO}_{3-\gamma}$  ferrite as well. A large width of the optical phonon bands of the Raman  $\text{La}_{1-x}\text{Sr}_x\text{FeO}_{3-\gamma}$  spectra testifies to the significantly disordered oxygen ferrite sublattice with a sufficient number of oxygen vacancies.

## 4. Conclusions

Summarizing the results obtained, we come to the following conclusions. The as-prepared sample and those annealed in vacuum have a rhombohedral structure except for one sample annealed at 650 °C. It has

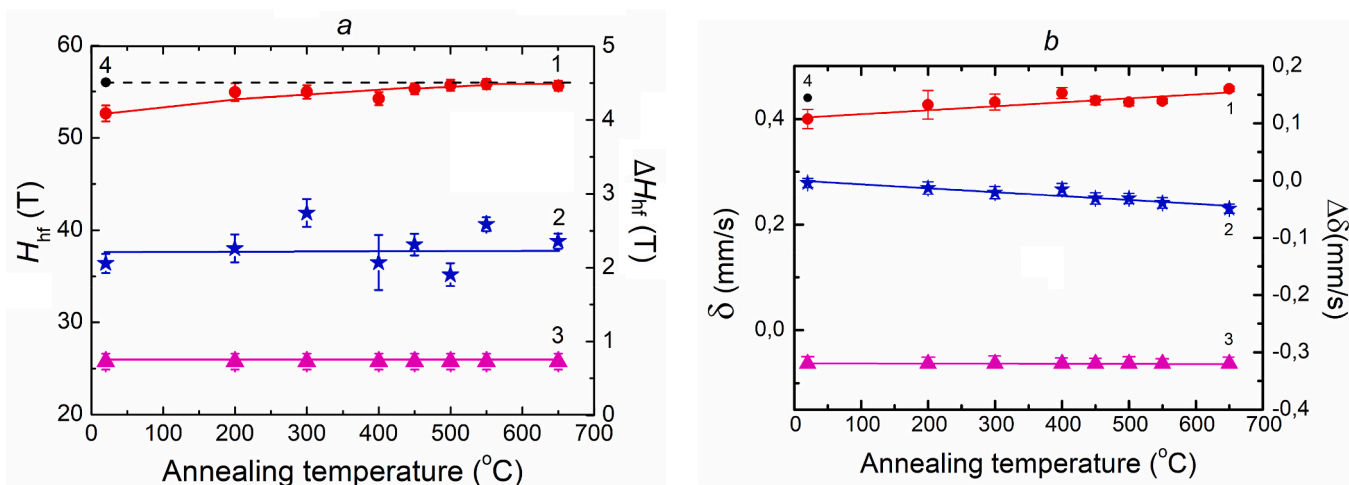


**Fig. 8.** The  $T_{\text{ann}}$  dependencies of the hyperfine parameters of the subspectra of  $\text{Fe}^{3+}$  and  $\text{Fe}^{4+}$  ions: (a)  $H_{\text{hf}}(\text{Fe}^{3+};0)$ ,  $\Delta H_{\text{hf}}(\text{Fe}^{3+})$ ,  $H_{\text{hf}}(\text{Fe}^{4+})$  and (b)  $\delta(\text{Fe}^{3+};0)$ ,  $\Delta\delta(\text{Fe}^{3+})$ ,  $\delta(\text{Fe}^{4+})$  as compared to the corresponding data for  $\text{LaFeO}_3$ . The Mössbauer parameters correspond to the 85-K spectra. 1 –  $H_{\text{hf}}(\text{Fe}^{3+};0)$ ,  $\delta(\text{Fe}^{3+};0)$ ; 2 –  $\Delta H_{\text{hf}}(\text{Fe}^{3+})$ ,  $\Delta\delta(\text{Fe}^{3+})$ ; 3 –  $H_{\text{hf}}(\text{Fe}^{4+})$ ,  $\delta(\text{Fe}^{4+})$ ; 4 –  $H_{\text{hf}}(\text{LaFeO}_3)$ ,  $\delta(\text{LaFeO}_3)$ . The lines drawn through the data points are guides for the eye.

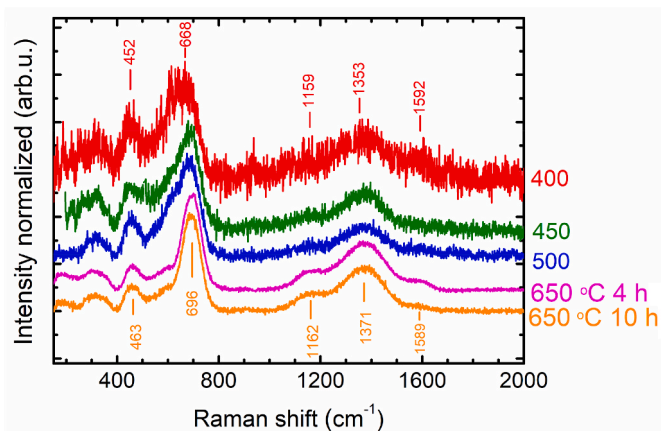


**Fig. 9.** Representative Raman spectra of the  $\text{La}_{0.5}\text{Sr}_{0.5}\text{FeO}_{3-\gamma}$  ferrites. The lowest spectrum corresponds to the sample annealed at  $650^\circ\text{C}$  for 10 h. The spectrum intensities were normalized to the amplitude of the peak at  $\sim 670\text{ cm}^{-1}$ . The annealing temperatures (in  $^\circ\text{C}$ ) for each spectrum are given at the right.

a cubic perovskite structure ( $Pm\bar{3}m$ ). The pseudocubic unit cell volume increases for the samples annealed in vacuum at  $200\text{--}500^\circ\text{C}$ ; it almost does not change at higher annealing temperatures. The changes in the structural parameters occur up to  $650^\circ\text{C}$ .

The as-prepared sample is paramagnetic at room temperature. Upon the oxygen loss under vacuum annealing, the magnetic contribution appears in addition to the paramagnetic fraction of the sample; its fraction increases with an increase in the annealing temperature. The quadrupole doublet associated with a paramagnetic state almost disappears in the Mössbauer spectra of the samples annealed at temperatures above  $450^\circ\text{C}$ .

The analysis of the Mössbauer spectra demonstrates that Fe ions are in an averaged-valence state at room temperature. This state is not observed in the 85-K spectra, which allows separating the subspectra of  $\text{Fe}^{3+}$  and  $\text{Fe}^{4+}$  ions, determining their relative areas, and calculating the amount of oxygen in the samples.

Based on the results that were obtained using three different methods and agree with each other, the following may be concluded on the nature of changes taking place in  $\text{La}_{0.5}\text{Sr}_{0.5}\text{FeO}_{3-\gamma}$ : the transformation of the valence state of Fe ions from  $4+$  up to complete  $\text{Fe}^{4+}$

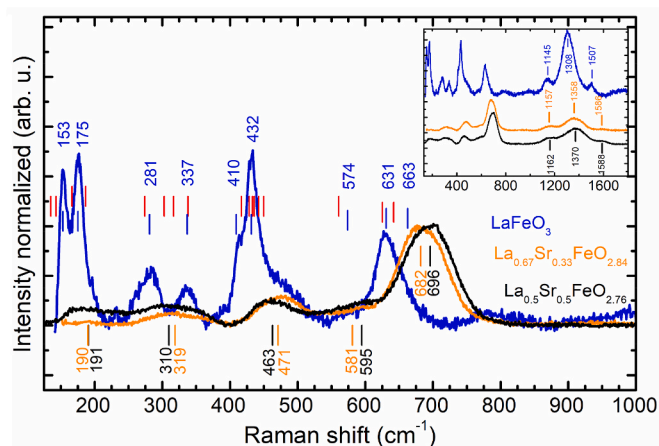


**Fig. 10.** Raman spectra of pure  $\text{LaFeO}_3$  and the substituted  $\text{La}_{1-x}\text{Sr}_x\text{FeO}_{3-\gamma}$  ferrites with Fe ions in a  $\text{Fe}^{3+}$  oxidation state. The spectrum intensities were normalized to the intensity of the peak in the frequency range of  $600\text{--}700\text{ cm}^{-1}$ . Red vertical bars denote the experimental positions of  $\text{LaFeO}_3$  peaks presented in Ref. [23]. The spectra for  $\text{La}_{0.67}\text{Sr}_{0.33}\text{FeO}_{2.84}$  and  $\text{LaFeO}_3$  were taken from Ref. [24]. The same spectra in the wide frequency range are shown in the inset. The exact sample compositions are given on the right side of the main panel. (For interpretation of the references to colour in this figure legend, the reader is referred to the Web version of this article.)

disappearance and an increase in the number of oxygen vacancies occur simultaneously in the vacuum annealing temperature range of  $200\text{--}500^\circ\text{C}$ . The annealing at  $500\text{--}650^\circ\text{C}$  leads to a significant decrease in the degree of distortion of the ferrite structure at a local level. The areas of the Mössbauer subspectra responsible for different oxygen environments of Fe ions are redistributed, and the fraction of non-distorted oxygen octahedral increases. Finally, the rhombohedral structure transforms into the cubic one.

#### Funding

This research did not receive any specific grant from funding agencies in the public, commercial, or not-for-profit sectors.

## Author statement

V. Sedykh: Supervision, Conceptualization, Investigation, Writing - Original Draft, Writing - Review & Editing, V. Rusakov: Conceptualization, Writing - Original Draft, O. Rybchenko: Investigation, Formal analysis, Writing - Review & Editing, M. Gapochka: Investigation, K. Gavrilicheva: Visualization, Formal analysis, O. Barkalov: Investigation, Formal analysis, Writing - Review & Editing, S. Zaitsev: Investigation, V. Kulakov: Formal Investigation.

## Data availability

No data was used for the research described in the article.

## Declaration of competing interest

The authors declare that they have no known competing financial interests or personal relationships that could have appeared to influence the work reported in this paper.

## Acknowledgments

Raman measurements were carried out on a spectrometer of the Center for Collective Using at the Osipyan Institute of Solid State Physics, Russian Academy of Sciences. This work was carried out within the framework of the State task of the Osipyan Institute of Solid State Physics of Russian Academy of Sciences <http://www.issp.ac.ru/main/index.php/ru/novosti-skryt/1696-7-2021-265.html>.

## References

- M.B. Salamon, M. Jaime, The physics of manganites: structure and transport, *Rev. Mod. Phys.* 73 (2001) 583–628, <https://doi.org/10.1103/REVMODPHYS.73.583>.
- By Y. Tokura (Ed.), *Colossal Magnetoresistive Oxides*, CRC Press, London, 2000, p. 280, <https://doi.org/10.1201/9781482287493>.
- E.A. Tugova, V.F. Popova, I.A. Zvereva, V.V. Gusarov, Phase diagram of the LaFeO<sub>3</sub>-LaSrFeO<sub>4</sub> system, *Glass Phys. Chem.* 32 (2006) 674–676, <https://doi.org/10.1134/S1087659606060137>.
- S. Petrović, A. Terlecki-Barčević, Lj. Karanović, P. Kirilov-Stefanov, M. Zdujić, V. Dondur, D. Paneva, I. Mitov, V. Rakić, LaMO<sub>3</sub> (M=Mg, Ti, Fe) perovskite type oxides: preparation, characterization and catalytic properties in methane deep oxidation, *Appl. Catal. B Environ.* 79 (2008) 186–198, <https://doi.org/10.1016/j.apcatb.2007.10.022>.
- S.N. Tijare, M.V. Joshi, P.S. Padole, P.A. Mangrulkar, S.S. Rayalu, N.K. Labhsetwar, Photocatalytic hydrogen generation through water splitting on nano-crystalline LaFeO<sub>3</sub> perovskite, *Int. J. Hydrogen Energy* 37 (2012) 10451–10456, <https://doi.org/10.1016/j.ijhydene.2012.01.120>.
- Z.-X. Wei, Y.-Q. Xu, H.-Y. Liu, C.-W. Hu, Preparation and catalytic activities of LaFeO<sub>3</sub> and Fe<sub>2</sub>O<sub>3</sub> for HMX thermal decomposition, *J. Hazard Mater.* 165 (2009) 1056–1061, <https://doi.org/10.1016/j.jhazmat.2008.10.086>.
- J. Faye, A. Baylet, M. Trentesaux, S. Royer, F. Dumeignil, D. Duprez, S. Valange, J.-M. Tatibouët, Influence of lanthanum stoichiometry in La<sub>1-x</sub>FeO<sub>3-δ</sub> perovskites on their structure and catalytic performance in CH<sub>4</sub> total oxidation, *Appl. Catal. B Environ.* 126 (2012) 134–143, <https://doi.org/10.1016/j.apcatb.2012.07.001>.
- Y. Shin, K.-Y. Doh, S.H. Kim, J.H. Lee, H. Bae, S.-J. Song, D. Lee, Effect of oxygen vacancies on electrical conductivity of La<sub>0.5</sub>Sr<sub>0.5</sub>FeO<sub>3-δ</sub> from first-principles calculations, *J. Mater. Chem. A* 8 (2020) 4784–4789, <https://doi.org/10.1039/C9TA12734H>.
- J.B. Yang, W.B. Yelon, W.J. James, Z. Chu, M. Kornecki, Y.X. Xie, X.D. Zhou, H. U. Anderson, A.G. Joshi, S.K. Malik, Crystal structure, magnetic properties, and Mössbauer studies of La<sub>0.6</sub>Sr<sub>0.4</sub>FeO<sub>3-δ</sub> prepared by quenching in different atmospheres, *Phys. Rev. B* 66 (2002), 184415.
- J. Goodenough, *Metallic oxides*, *Prog. Solid State Chem.* 5 (1971) 145–399, [https://doi.org/10.1016/0079-6786\(71\)90018-5](https://doi.org/10.1016/0079-6786(71)90018-5).
- S. Phokha, S. Pinitsoontorn, S. Rujirawat, S. Maensiri, Polymer pyrolysis synthesis and magnetic properties of LaFeO<sub>3</sub> nanoparticles, *Phys. B Condens. Matter* 476 (2015) 55–60, <https://doi.org/10.1016/j.physb.2015.07.021>.
- J.B. Goodenough, *Physical chemistry: magnetism and the chemical bond*, *Science* 143 (3601) (1964) 33–34, <https://doi.org/10.1126/science.143.3601.33.b>.
- U. Shimony, J.M. Knudsen, Mössbauer studies on iron in the perovskites La<sub>1-x</sub>Sr<sub>x</sub>FeO<sub>3</sub> (0 << x << 1), *Phys. Rev.* 144 (1966) 361–366, <https://doi.org/10.1103/PhysRev.144.361>.
- J.-C. Grenier, N. Ea, M. Pouchard, Mm Abou-Sekkina, Proprietés électriques et magnétiques des ferrites oxydes La<sub>1-x</sub>Sr<sub>x</sub>FeO<sub>3-y</sub>, *Mater. Res. Bull.* 19 (1984) 1301–1309, [https://doi.org/10.1016/0025-5408\(84\)90192-2](https://doi.org/10.1016/0025-5408(84)90192-2).
- P.D. Battle, T.C. Gibb, S. Nixon, A study of the ordering of oxygen vacancies in the nonstoichiometric perovskite Sr<sub>2</sub>LaFe<sub>3</sub>O<sub>8+y</sub> by Mössbauer spectroscopy and a comparison with SrFeO<sub>3-y</sub>, *J. Solid State Chem.* 79 (1989) 75–85, [https://doi.org/10.1016/0022-4596\(89\)90252-1](https://doi.org/10.1016/0022-4596(89)90252-1).
- T.M. Rearick, G.L. Catchen, J.M. Adams, Combined magnetic-dipole and electric-quadrupole hyperfine interactions in rare-earth orthoferrite ceramics, *Phys. Rev. B* 48 (1993) 224–238, <https://doi.org/10.1103/PhysRevB.48.224>.
- P.K. Gallagher, J.B. MacChesney, D.N.E. Buchanan, Mössbauer effect in the system SrFeO<sub>2.5-3.0</sub>, *J. Chem. Phys.* 41 (1964) 2429–2434, <https://doi.org/10.1063/1.1726282>.
- P.K. Gallagher, J.B. MacChesney, Mössbauer effect in the system Sr<sub>1-x</sub>La<sub>x</sub>FeO<sub>3</sub>, *Symp. Faraday Soc.* 1 (1967) 40–47, <https://doi.org/10.1039/SF9670100040>.
- R.B. da Silva, J.M. Soares, José A.P. da Costa, J.H. de Araújo, A.R. Rodrigues, F.L. A. Machado, Local iron ion distribution and magnetic properties of the perovskites La<sub>1-x</sub>Sr<sub>x</sub>FeO<sub>3-y</sub>, *J. Magn. Magn. Mater.* 466 (2018) 306–310, <https://doi.org/10.1016/j.jmmm.2018.07.040>.
- A. Fossdal, M. Menon, I. Waernhus, K. Wiik, M.-A. Einarsrud, T. Grande, Crystal structure and thermal expansion of La<sub>1-x</sub>Sr<sub>x</sub>FeO<sub>3-δ</sub> materials, *J. Am. Ceram. Soc.* 87 (2004) 1952–1958, <https://doi.org/10.1111/j.1151-2916.2004.tb06346.x>.
- G. Li, L. Li, M. Zhao, The study of <sup>57</sup>Fe Mössbauer spectra for La<sub>0.7</sub>Sr<sub>0.3</sub>FeO<sub>3-δ</sub> with different structure, *Phys. Status Solidi B* 197 (1996) 165–172, <https://doi.org/10.1002/pspb.2221970123>.
- H. Yamamura, R. Kiriyama, Oxygen vacancies in the perovskite-type ferrites. II. Mössbauer effect in the SrFeO<sub>2.5</sub>-LaFeO<sub>3</sub> solid-solution system, *Bull. Chem. Soc. Jpn.* 45 (1972) 2702–2708, <https://doi.org/10.1246/bcsj.45.2702>.
- M.C. Weber, M. Guennou, H.J. Zhao, J. Íñiguez, R. Vilarinho, A. Almeida, J. A. Moreira, J. Kreisel, Raman spectroscopy of rare-earth orthoferrites RFeO<sub>3</sub> (R = La, Sm, Eu, Gd, Tb, Dy), *Phys. Rev. B* 94 (2016), 214103, <https://doi.org/10.1103/PhysRevB.94.214103>.
- V. Sedykh, O. Rybchenko, V. Rusakov, S. Zaitsev, O. Barkalov, E. Postnova, T. Gubaidulina, D. Pchelina, V. Kulakov, Role of Fe atom valence states and oxygen vacancies in substituted lanthanum ferrite La<sub>0.67</sub>Sr<sub>0.33</sub>FeO<sub>3-y</sub>, *J. Phys. Chem. Solid.* 171 (2022), 111001 <https://doi.org/10.1016/j.jpcs.2022.111001>.
- V.D. Sedykh, O.G. Rybchenko, A.N. Nekrasov, I.E. Koneva, V.I. Kulakov, Effect of the oxygen content on the local environment of Fe atoms in anion-deficient SrFeO<sub>3-δ</sub>, *Phys. Solid State* 61 (2019) 1099–1106, <https://doi.org/10.1134/S1063783419060210>.
- M.E. Matsnev, V.S. Rusakov, SpectrRelax: an application for Mössbauer spectra modeling and fitting, in: *AIP Conf. Proc.*, vol. 1489, American Institute of Physics AIP, 2012, pp. 178–185, <https://doi.org/10.1063/1.4759488>.
- N.V. Zaitseva, Ya.V. Kopelevich, I.I. Kochina, V.V. Lemanov, P.P. Snyrnkov, Lattice parameters and electrical conductivity of YBa<sub>2</sub>Cu<sub>3</sub>O<sub>x</sub> ceramic vs oxygen content, *Fiz. Tverd. Tela* 33 (1991) 569–574, <https://www.mathnet.ru/eng/ft/v33/i2/p569>.
- V. Sedykh, V.Sh. Shekhtman, I.I. Zverkova, A.V. Dubovitskii, V.I. Kulakov, Reversibility of structure phase transitions in LaMnO<sub>3+δ</sub> manganite under heat treatment, *Phys. C Supercond.* 433 (2006) 189–194, <https://doi.org/10.1016/j.physc.2005.10.013>.
- P.D. Battle, T.C. Gibb, S. Nixon, A study of charge disproportionation in the nonstoichiometric perovskite Sr<sub>2</sub>LaFe<sub>3</sub>O<sub>8+y</sub> by Mössbauer spectroscopy, *J. Solid State Chem.* 77 (1988) 124–131, [https://doi.org/10.1016/0022-4596\(88\)90099-0](https://doi.org/10.1016/0022-4596(88)90099-0).
- G.A. Sawatzky, F. Van Der Woude, Covalency effects in hyperfine interactions, *J. Phys. Colloq.* 35 (1974), <https://doi.org/10.1051/jphyscol:1974605>. C6-47-C6-60.
- M. Takano, J. Kawachi, N. Nakanishi, Y. Takeda, Valence state of the Fe ions in Sr<sub>1-y</sub>La<sub>y</sub>FeO<sub>3</sub>, *J. Solid State Chem.* 39 (1981) 75–84, [https://doi.org/10.1016/0022-4596\(81\)90304-2](https://doi.org/10.1016/0022-4596(81)90304-2).
- S.E. Dann, D.B. Currie, M.T. Weller, M.F. Thomas, A.D. Al-Rawwas, The effect of oxygen stoichiometry on phase relations and structure in the system La<sub>1-x</sub>Sr<sub>x</sub>FeO<sub>3-δ</sub> (0 ≤ x ≤ 1, 0 ≤ δ ≤ 0.5), *J. Solid State Chem.* 109 (1994) 134–144, <https://doi.org/10.1006/JSSC.1994.1083>.
- A.D. Al-Rawwas, C.E. Johnson, M.F. Thomas, S.E. Dann, M.T. Weiler, Mössbauer studies on the series La<sub>1-x</sub>Sr<sub>x</sub>FeO<sub>3</sub>, *Hyperfine Interact.* 93 (1994) 1521–1529, <https://doi.org/10.1007/BF02072903>.
- Danjela Kušćer, Darko Hanzel, Janez Holc, Marko Hrovat, Kolar Drago, Defect structure and electrical properties of La<sub>1-y</sub>Sr<sub>y</sub>Fe<sub>1-x</sub>Al<sub>x</sub>O<sub>3.85</sub>, *J. Am. Ceram. Soc.* 84 (5) (2001) 1148–1154, <https://doi.org/10.1111/j.1151-2916.2001.tb00803.x>.
- J. Andreasson, J. Holmlund, C.S. Kneel, M. Käll, L. Börjesson, S. Naler, J. Bäckström, M. Rübhausen, A.K. Azad, S.-G. Eriksson, Franck-Condon higher order lattice excitations in the LaFe<sub>1-x</sub>Cr<sub>x</sub>O<sub>3</sub> (x = 0, 0.1, 0.5, 0.9, 1.0) perovskites due to Fe-Cr charge transfer effects, *Phys. Rev. B* 75 (2007), 104302, <https://doi.org/10.1103/PhysRevB.75.104302>.
- A.S. Anokhin, A.G. Razumnaya, V.I. Torgashev, V.G. Trotsenko, Yu.I. Zuyuk, A. A. Bush, V.Ya. Shkuratov, B.P. Gorshunov, E.S. Zhukova, L.S. Kadyrov, G. A. Komandin, Dynamic spectral response of solid solutions of the bismuth-strontium ferrite Bi<sub>1-x</sub>Sr<sub>x</sub>FeO<sub>3-δ</sub> in the frequency range 0.3–200 THz, *Phys. Solid State* 55 (2013) 1417–1430, <https://doi.org/10.1134/S1063783413070032>.
- S. Manzoor, S. Husain, V. Raghavendra Reddy, Epitaxial LaFeO<sub>3</sub> and LaFe<sub>0.75</sub>Nb<sub>0.25</sub>O<sub>3</sub> thin films on SrTiO<sub>3</sub> (STO) (100) substrate: structural studies and high energy magnon excitations, *Appl. Phys. Lett.* 113 (2018), 072901, <https://doi.org/10.1063/1.5025247>.
- O.I. Barkalov, S.V. Zaitsev, V.D. Sedykh, Strontium ferrite SrFeO<sub>3-δ</sub> (2.50 ≤ δ ≤ 2.87) studied by Raman and Mössbauer spectroscopy, *Solid State Commun.* 354 (2022), 114912, <https://doi.org/10.1016/j.ssc.2022.114912>.